FISEVIER

### Contents lists available at ScienceDirect

## Applied Catalysis A, General

journal homepage: www.elsevier.com/locate/apcata



# Impacts of calcination on surface-clean supported nanoparticle catalysts



Kristin Bryant<sup>a</sup>, Christy Wheeler West<sup>b</sup>, Steven R. Saunders<sup>a,c,\*</sup>

- <sup>a</sup> The Gene and Linda Voiland School of Chemical Engineering and Bioengineering, Washington State University, Pullman, WA, 99164, United States
- b Department of Chemical and Biomolecular Engineering, University of South Alabama, Mobile, AL, 36688, United States
- <sup>c</sup> Department of Chemistry, Washington State University, Pullman, WA, 99164, United States

#### ARTICLE INFO

Keywords: Switchable surfactants Nanomaterials Catalysis Calcination

#### ABSTRACT

Traditional methods of preparing size-controlled supported nanoparticle catalysts typically require the use of stabilizing ligands that passivate the nanoparticle surface to prevent overgrowth and aggregation. The presence of these ligands on catalytic surfaces can be detrimental to activity and are typically removed via a high-temperature annealing step, which ultimately results in changes to nanoparticle morphology and thus, reduced activity. We previously demonstrated that silylamine switchable surfactants can be used to synthesize and deposit highly active nanoparticles on to a support surface while preserving monodispersity. Here, we demonstrate using XPS that supported nanoparticles prepared in this manner are surface-clean after deposition, eliminating the need for traditional activation steps. Further, it is shown that even low-temperature calcinations have detrimental effects on the catalyst properties including changes in nanoparticle morphology that result in a significant decrease in activity, a change in surface hydrophilicity, a change in activation energy, and results in the formation of an induction time when utilized in the hydrogenation of 4-nitrophenol. While calcination remains a widely used method of catalyst activation, the detrimental effects of high temperatures on catalyst properties are often overlooked.

### 1. Introduction

The vast majority of existing size-controlled supported nanoparticle syntheses employ capping agents to inhibit nanoparticle overgrowth and aggregation; however, the presence of these capping agents can be detrimental to catalytic activity and therefore are typically removed via a high-temperature calcination, which ultimately results in unfavorable changes to the active phase. The development of colloidal synthesis methods allows for the precise tailoring of structural characteristics such as the size and shape of nanoparticles through the use of molecules that chemisorb to the nanoparticle surface often denoted as surfactants. ligands or capping agents [1-5]. The adsorption of capping agents on nanoparticle surfaces can saturate the surface and stabilize the nanoparticles through steric or electrostatic repulsion, protecting the nanoparticles from agglomeration and growth. While stabilizing molecules are necessary to control size and monodispersity during synthesis, these molecules typically have negative impacts on catalyst properties. Stabilizing agents chemisorbed to surface of the metallic nanoparticle limit active site availability and affect the local reaction environment, and thus surface-mediated properties such as catalytic activity [6-15].

Ligands may compete with reactants for adsorption sites during catalysis and significantly hinder catalytic performance in even minute quantities [16–18]. Further, the presence of capping agents adds complexity to the system, such as interactions among the capping molecules and reagents, charge transfer at the organic ligand-metal interface, and non-uniform coverage of the capping agent on the nanoparticle surface [19]. Additionally, variation in capping agent coverage density may lead to problems with reproducibility in catalytic studies. It has been shown that removal of stabilizing ligands typically enhances the catalytic activity of colloidal nanoparticles [20–23].

Perhaps the most widely used ligand removal technique is thermal degradation of ligands through a high-temperature calcination. While effective in removing bound surface species, it is reported in the literature that exposure to high temperatures increases nanoparticle mobility and Ostwald ripening, typically leading to polydisperse nanoparticle populations [24–27]. Further, while size effects of calcination are well documented, investigations into other possible detrimental effects of calcination on catalyst properties are absent from the literature

Alternative methods of ligand removal aimed at preserving

E-mail address: steven.r.saunders@wsu.edu (S.R. Saunders).

Abbreviations: RevIL, reversible ionic liquid; SwiS, switchable surfactant; APTES, 3-aminopropyltriethylsilane

<sup>\*</sup> Corresponding author at: The Gene and Linda Voiland School of Chemical Engineering and Bioengineering, Washington State University, Pullman, WA, 99164, United States.

nanoparticle morphology have been reported such as solvent extractions [28], chemical treatments [29-31], and plasma treatments [32]. While these methods have the ability to effectively remove ligands to some extent, in many cases the effects on the nanoparticle surface chemistry are poorly characterized. In some cases the ligands can be decomposed into smaller fragments with heat or light followed by removal with a gas flow such as in UV-ozone irradiation; however, this process can cause size changes, residual ligands can be left behind, and often the surface atoms become partially oxidized [22,33-39]. Partial or incomplete decomposition of ligands during thermal or UV-ozone treatment may generate coke or other poisons that can deactivate the catalyst [40]. Ligand exchange may be used to replace ligands with small molecules that have much lower boiling points and competitive capping abilities. These can then be removed easily with washing or vacuum evaporation; however, ligand exchange and washing steps often result in leaching of base metals [41]. Despite its downfalls, calcination remains a widely used method of ligand removal due to the lack of viable alternatives. The traditional methods used to remove stabilizing ligands cannot preserve the nanoparticle surface and, as such, there is a possibility that optimal catalytic surfaces exist that cannot be accessed using classical methods.

Previously, we demonstrated a novel method to prepare highly-active, size-controlled supported nanoparticles using a switchable surfactant (SwiS) system [42]. It was shown that silylamine reversible ionic liquids (RevIL) can be converted between molecular and ionic forms via reaction with CO2 (see Scheme 1). Upon addition of an alkane, the ionic form of the RevIL functions as a SwiS that can be used to stabilize and template nanoparticles during synthesis. Upon reversal of the ionic liquid via removal of CO2, the nanoparticles directly deposit on to the support surface with no change to nanoparticle size. It was demonstrated that supported nanoparticle catalysts prepared with SwiS were more active prior to calcination than their traditionally prepared counterparts after calcination. Analysis with Fourier transform infrared spectroscopy showed that the molecular silvlamine interacts with the catalyst surface after deposition and washing; however, it was unclear if the silylamine stabilizes the nanoparticle surface or interacts only with the support. In this work, we demonstrate that supported nanoparticles prepared with SwiS are surface-clean after deposition and are significantly more active prior to attempted removal of the molecular species via a low-temperature calcination. Further, we show that calcination of the surface-clean supported nanoparticles has detrimental effects on catalyst characteristics beyond those associated with nanoparticle morphology changes.

### 2. Experimental section

### 2.1. Materials

Hydrogen tetrachloroaurate tri-hydrate (HAuCl<sub>4</sub>·3H<sub>2</sub>O; 49% Au) was obtained from Sigma Aldrich. Sodium borohydride (NaBH<sub>4</sub>; > 97%), and silica (SiO<sub>2</sub>; 0.060-0.2 mm) were acquired from Alfa Aesar. N-hexane ( $C_6H_{14}$ ; > 95%) and hydrochloric acid (HCl; 36.5–38%) were purchased from J.T. Baker. 4-Nitrophenol ( $C_6H_5NO_3$ ; 98%) was acquired from Acros Organics. Nitric acid (HNO<sub>3</sub>; TraceMetal grade) was obtained from Fisher Chemical. Clinical laboratory reagent water (CLRW) – Type 1 was obtained from Thermo Fisher Scientific. 200 mesh Carbon Formvar-coated copper grids were obtained from Ted Pella. Toluene was dried over molecular sieves before use. All other

$$\begin{array}{c|c}
2 & -Si & NH_2 & +CO_2 \\
\hline
& -CO_2 & -Si & NH_3^+ - O & H \\
& -CO_2 & -Si & NH_3^+ - O & N
\end{array}$$

Scheme 1. The silylamine molecular liquid reacts reversibly with  ${\rm CO}_2$  to form an ionic liquid.

materials were used without additional purification.

#### 2.2. Nanoparticle synthesis and deposition

Monodisperse gold nanoparticles were synthesized using a reversible ionic liquid (RevIL) as demonstrated in a previous work [42,43]. Details regarding the synthesis of the RevIL is outlined in the Supporting Information. To prepare the nanoparticles, HAuCl4 (0.044 mmol) and hexane (0.078 mol) were added to the ionic liquid (5 mmol, 3-aminopropyltriethylsilane, APTES). The mixture was stirred until the gold precursor had completely dissolved. 200  $\mu L$  of aqueous NaBH4 (0.1 M) was added to the reaction mixture while stirring at 400 rpm. The reaction was stirred for 1 h.

The gold nanoparticles were deposited on to non-porous silica gel following a method previously demonstrated [42]. Briefly,  $10.5\,\mathrm{mL}$  of the as-prepared nanoparticle solution was added to a flask containing 12 g of silica and 400 mL of hexane. The reaction mixture was stirred at 400 rpm for the duration of deposition. The flask was connected to a reflux column and the reaction was heated to reflux conditions (~69 °C). Refluxing continued until deposition was complete, indicated by a color change of the supernatant from purple to clear (~30 min), at which point the reaction mixture was cooled to room temperature. The supernatant was removed and discarded. The supported nanoparticles were washed with hexane and dried in a vacuum oven set at 45 °C.

#### 2.3. Low-temperature calcination

The supported nanoparticles were calcined in air for six unique time lengths. For each calcination, the temperature was increased from room temperature at 5 °C/min to 230 °C. The temperature was held at 230 °C for 0, 15, 30, 60, 120, or 180 min yielding seven total samples. 230 °C was chosen as the calcination temperature as it is just above the boiling temperature of the neat molecular APTES.

### 2.4. Nanoparticle characterization

Gold loading of the supported nanoparticle samples was measured using inductively-coupled plasma mass spectroscopy (ICP-MS) on an Agilent 7700 at Washington State University in the Peter Hooper GeoAnalytical Lab. The catalyst samples were digested in aqua-regia and diluted to  $2\%\ HNO_3$  for quantification.

Transmission electron microscopy (TEM) was used to determine nanoparticle size utilizing an FEI Tecnai G2 T20 Twin TEM with an operating voltage of 200 kV. The supported nanoparticles were suspended in hexane and drop cast on to grids. ImageJ software was used for image analysis. At least 300 nanoparticles were manually sized to ensure statistical significance by measuring the longest nanoparticle axis.

Attenuated total reflectance Fourier transform infrared (ATR-FTIR) spectroscopy on a ThermoScientific Nicolet IS10 was used to characterize the supported nanoparticles before and after calcination. Spectra were acquired from  $650\,\mathrm{cm}^{-1}$  to  $4000\,\mathrm{cm}^{-1}$ .

Surface analysis was performed with X-ray photoelectron spectrometry (XPS) using a spectrometer equipped with a Kratos AXIS-165 monochromatized Al  $K_{\alpha}$  X-ray anode (1486.6 eV) and with a power of 202 W. For the XPS measurements, the samples were cleaned by Ar $^+$  sputtering to remove contamination. The ion gun parameters used were 15 mA @ 4 kV and sputter time of 1 min. The carbon C 1S peak at 285 eV was used as a reference for charge correction. The spectra were analyzed using commercial CasaXPS software. For each analysis, the Shirley background was taken and Gaussian (70%) – Lorentzian (30%) profiles were used for each component. The best-fit analysis was performed to minimize  $\chi^2.$ 

Scheme 2. Gold catalyzed hydrogenation of 4-nitrophenol.

### 2.5. Evaluation of catalytic activity

The catalytic activity of the supported nanoparticles was evaluated before and after calcination by utilizing them in the catalyzed reduction of 4-nitrophenol to 4-aminophenol (see Scheme 2) using a method previously developed [42,44]. For each catalytic test, an aqueous reaction solution containing 0.1 mM 4-nitrophenol and 0.1 M NaBH<sub>4</sub> was prepared under stirring at 300 rpm at room temperature. An aliquot of the reaction mixture was placed in a 1 cm path length, polystyrene cuvette and the absorbance spectrum measured (Agilent Cary 100 spectrophotometer) to obtain an initial absorbance of 4-nitrophenolate at 400 nm. The reaction was initiated by adding the catalyst (approximately 0.05 g) to the mixture and a timer started. Samples were taken at regular intervals (30-seconds), filtered through a syringe filter (0.2 µm nylon membrane) to stop the reaction, placed in a cuvette, and the absorbance spectrum measured. All catalytic tests were performed in triplicate.

### 2.6. Activation energy determination

The activation energy of the pre-calcined supported nanoparticles and those calcined at 230  $^{\circ}$ C for 180 min was evaluated. The activation energy tests were conducted following the same manner as the catalytic activity tests (see Scheme 2). The catalytic tests were run at four temperatures roughly 10  $^{\circ}$ C apart between 10  $^{\circ}$ C and 60  $^{\circ}$ C in order to evaluate activation energies of the two catalyst samples.

### 3. Results and discussion

Surface analysis performed previously on silica-supported gold nanoparticles prepared with SwiS indicated the presence of the APTES molecular species interacting with the catalyst surface after deposition and washing; however, it was unclear whether the species interacts with the nanoparticle or only the support surface [42]. Here, the nanoparticles from a single synthesis and deposition were calcined for six unique time lengths to determine if the adsorbed molecular APTES can be removed without affecting catalyst characteristics. The size, catalytic activity, and activation energy of the calcined catalyst samples were compared to those of the pre-calcined sample.

### 3.1. Effect of low-temperature calcination on nanoparticle size

Representative TEM micrographs and size distributions are shown in Fig. 1 and all average nanoparticle sizes are displayed in Table 1. Prior to calcination at 230 °C, the average size of the supported gold nanoparticles was 3.3  $\pm$  0.5 nm. An apparent change in nanoparticle size and distribution resulted after the low-temperature calcination at all conditions tested. A 9% size increase (3.3  $\pm$  0.5 nm to 3.6  $\pm$  0.7 nm) was seen after a calcination with no hold; however, there is no statistically significant difference (as determined by a single-factor ANOVA analysis and Tukey HSD [45] with p < 0.01) for calcinations up to and including the 60 min hold. A statistically significant increase in average size occurs for the 120 min calcination where the average diameter showed a 45% increase (3.3  $\pm$  0.5 nm to 4.8  $\pm$  2.0 nm) compared to the pre-calcined sample. No statistically significant change in size occurs between the 120 min and 180 min

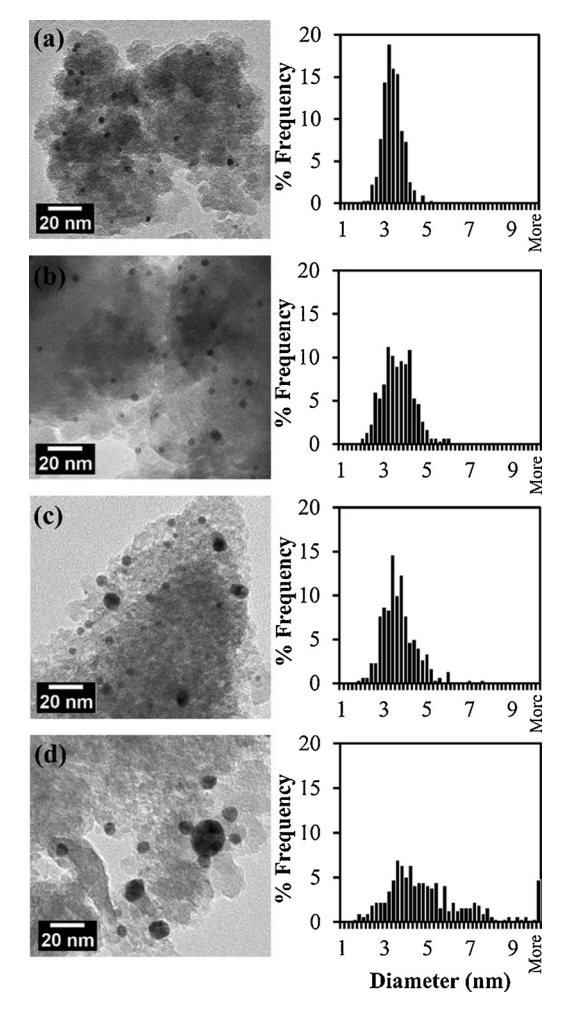


Fig. 1. TEM micrographs and size distributions of gold nanoparticles supported on  $SiO_2$  prepared with SwiS (a) before calcination, (b) calcined, no hold, (c) calcined, 60 min hold, and (d) calcined, 180 min hold.

Table 1 Nanoparticle diameters, gold loading, and geometric estimation of surface atoms/g catalyst for all catalyst samples. Hold time refers to the length of calcination at  $230\,^{\circ}$ C.

	nanoparticle diameter (nm)	gold loading (mg Au/g catalyst)	surface atoms per g catalyst x10 <sup>17</sup>
pre-calcined	$3.3 \pm 0.5$	$0.255 \pm 0.003$	1.3
no hold	$3.6 \pm 0.7$	$0.299 \pm 0.013$	1.4
15 min hold	$3.5 \pm 0.9$	$0.320 \pm 0.010$	1.4
30 min hold	$3.6 \pm 0.9$	$0.313 \pm 0.008$	1.4
60 min hold	$3.6 \pm 0.9$	$0.362 \pm 0.004$	1.6
120 min hold	$4.8 \pm 2.0$	$0.362 \pm 0.004$	0.96
180 min hold	$5.0 \pm 2.4$	$0.363 \pm 0.005$	0.84

calcinations. The single-factor ANOVA analysis with Tukey HSD for all catalyst samples is shown in the Supporting Information. While the calcination at 230  $^{\circ}$ C is considerably low compared to traditional calcination temperatures, which are typically between 500  $^{\circ}$ C and 800  $^{\circ}$ C [46–48], large changes in nanoparticle morphology still occur.

### 3.2. Surface analysis

FTIR analysis was performed on the supported nanoparticles before and after calcination and the resulting spectra are shown in Fig. 2. Molecular APTES is clearly present prior to calcination indicated by the  ${\rm CH_2}$  peaks at 2900 and 1450 cm $^{-1}$  as well as the N–H stretching region

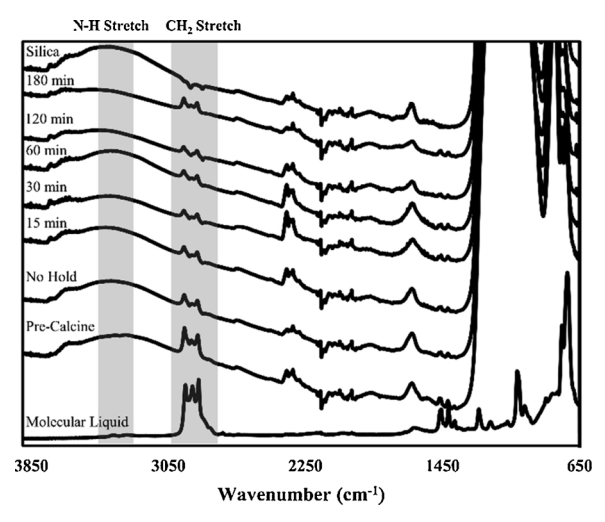


Fig. 2. FTIR spectra of the supported nanoparticles before and after calcination, the molecular liquid, and the silica support. No Hold –  $180\,\mathrm{min}$  refer to the duration of calcination at  $230\,^{\circ}\mathrm{C}$ .

at  $3250\,\mathrm{cm^{-1}}$  to  $3370\,\mathrm{cm^{-1}}$ . While the  $\mathrm{CH_2}$  peaks are visible in every sample before and after calcination, the N-H stretching band is only apparent in the molecular liquid and pre-calcination spectra likely due to the broad overlapping water adsorption peak from 3100 cm<sup>-1</sup> to 3500 cm<sup>-1</sup> and the weakening N-H signal as some of the molecular APTES is removed. The CH2 stretching band is absent in the silica spectrum indicating the CH2 present on the samples can be attributed to molecular APTES remaining on the catalyst surface. It is reported in the literature that when an amine is bound to the gold nanoparticle surface there is a complete absence of this characteristic N-H stretch [49]; however, due to the broad overlapping water peak, we are unable to confirm or deny the presence of an amine bound to the gold surface using FTIR. While this shows that the low-temperature calcination does not completely remove the molecular liquid from the catalyst surface, further characterization is needed to define the gold nanoparticle surface.

XPS was used to analyze the catalyst surface and determine the interaction between the Au nanoparticles and the molecular APTES after deposition and washing. Fig. 3 shows representative XPS spectra of Au 4f and N 1s photoelectrons of the pre- and post-calcination supported nanoparticles. Prior to calcination, it appears that three separate entities are present within the N 1s band as shown in Fig. 3(a). The peaks at 398.7, 399.9, and 402.3 eV are attributed to Si-NH2 [50], C-NH<sub>2</sub> [51], and NSiO<sub>2</sub> [52], respectively, indicating the molecular liquid amine is interacting with the silica surface. After calcination, the peak attributed to NSiO2 is absent but peaks corresponding to Si-NH2 and C-NH<sub>2</sub> remain, still indicating the molecular liquid interacts with the silica surface. Although the molecular amine remains on the surface postcalcination, the peak intensity ratio of gold to nitrogen increases from 0.21 before calcination to 0.31 after calcination demonstrating that some nitrogen (likely associated with the molecular APTES) is removed during calcination at 230 °C. Further analysis of the Si 2p band is needed to confirm the exact nitrogen interactions; however, there is no indication in the N 1s spectra that interactions between Au and N exist. The N 1s peak for amine-stabilized gold nanoparticles would appear near 401.1 eV [53]. Prior to calcination the Au 4f doublet band has binding energies of 87.8 eV and 84.1 eV (see Fig. 3(c)) corresponding to the Au 4f<sub>5/2</sub> and Au 4f<sub>7/2</sub> peaks, respectively which are in good agreement with literature values of zero valent gold [53-55]. These characteristic Au peaks are an indication that only a single gold interaction is present in the pre-calcined sample. From this data, we can conclude that the supported gold nanoparticles are bare and the molecular APTES is not bound to catalytic active sites prior to calcination. These findings support our initial hypothesis that nanoparticles are destabilized when the APTES RevIL is reversed to molecular form via thermal elimination of  $\rm CO_2$ , releasing surface-clean nanoparticles that directly deposit on to the support surface. While the nitrogen species adsorbed on the support surface is not removed by calcination at 230 °C, catalysis is likely not significantly hindered by its presence as the active sites are bare. After calcination, the Au 4f signal intensity decreases by roughly 20% indicating nanoparticle agglomeration [56]; however, the peak positions do not shift showing zero valent gold remains on the surface after calcination. The gold-to-carbon peak intensity ratio increases from roughly 0.18 prior to calcination to 0.25 after calcination (see Figure S3 of the Supporting Information) indicating that carbon (associated with the APTES) is removed during calcination.

### 3.3. Gold loading

Gold loading values were calculated for all catalyst samples before and after calcination based on ICP-MS data and are shown in Table 1 above. The post-calcination gold loading values are larger than the precalcination loading in every case. This increase in loading is an indication that at least one species is removed during calcination and likely a combination of water and molecular APTES. There is a very small change in loading for calcination times of 0-30 minutes, however; more substantial mass loss (increased Au loading) occurs at 60 min. This observation is consistent with the removal of two distinct species, one that occurs after the no hold calcination and one that occurs after the 60 min calcination. Changes in gold loading are small between 60 and 180 min calcinations. While species differentiation is not possible with thermogravimetric analysis due to broad overlapping transitions (Figure S2 of the Supporting Information), water is present on the precalcined catalyst (shown by FTIR) and would be removed from the surface during the thermal treatment in addition to the APTES removal indicated by XPS.

### 3.4. Effect of calcination at 230 °C on catalytic activity

While a low-temperature calcination at 230 °C does not completely remove the nitrogen species from the catalyst support here, we can evaluate the effect of a low-temperature calcination on monodisperse, surface-clean nanoparticles, which is generally not possible with traditional synthesis methods. Apparent rate constants obtained from catalytic testing in the 4-nitrophenol reduction were converted to specific rate constants using gold loading values, shown in Fig. 4. These values are used for the analysis of total gold mass utilization. Calcination at 230 °C results in a large decrease in specific rate constant. We observe a drastic drop in catalytic activity between the no hold and 15 min calcinations. Catalytic activity decreases by roughly 65% between the no hold and 15 min calcinations. No apparent changes in specific rate are seen after the 15 min calcination.

To compare fundamental catalysis, specific rate constants were converted to turnover frequency (TOF). Quantification of gold nanoparticle surface area is difficult to achieve with experimental methods and, as such, the number of accessible metallic surface atoms per gram of total catalyst was estimated geometrically based on gold loading, average nanoparticle sizes, and population polydispersity to obtain consistent estimations of available surface area (see Table 1). The calculation method for the number of surface atoms per gram of catalyst is shown in the Supporting Information. Here turnover frequency is defined as

$$TOF = \frac{n_{4NP}}{n_{Av. Surf} \cdot t}$$

where  $n_{4NP}$  is the number of moles of 4-nitrophenol consumed,  $n_{Au\_Surf}$  is the moles of gold surface atoms, and t is the time length of the reaction. For each TOF calculation, the conversion was approximately 60% and the time length of the reaction refers to the portion in which

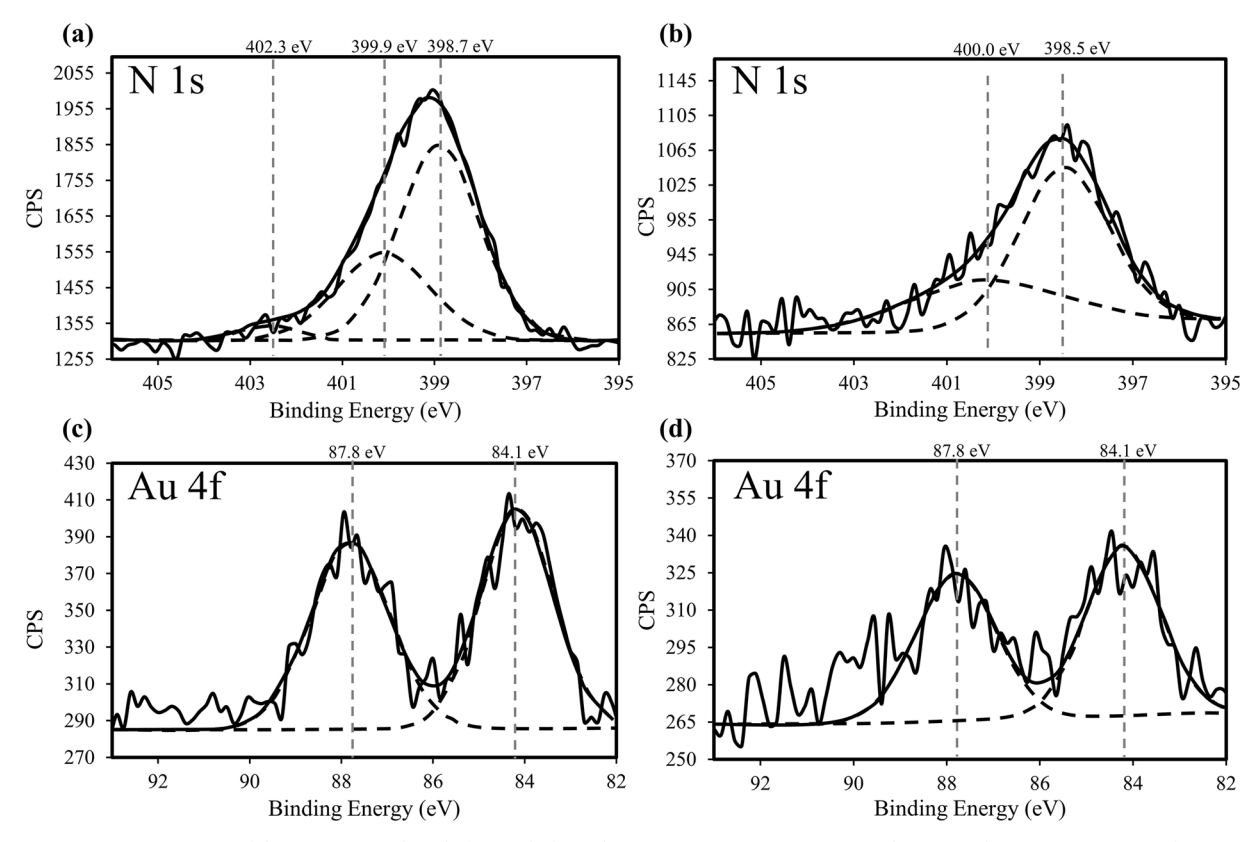


Fig. 3. Representative XPS spectra of the Au/SiO<sub>2</sub> catalysts before and after calcination at 230 °C. (a) N 1s pre-calcination, (b) N 1s post 60 min calcination, (c) Au 4f pre-calcination, and (d) Au 4f post 60 min calcination.

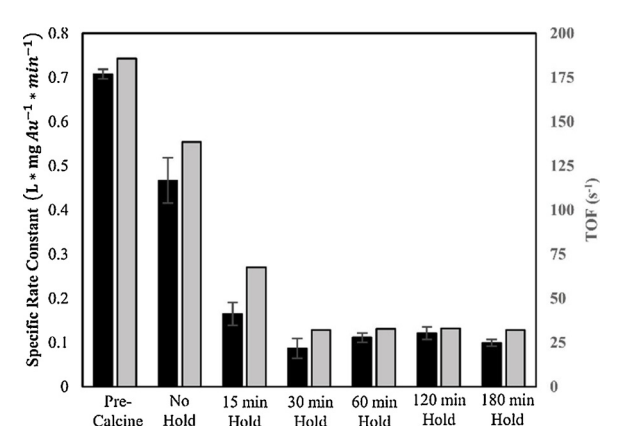


Fig. 4. Specific rate constants and turnover frequencies for all catalyst samples.

pseudo first-order kinetics can be assumed (i.e. excluding any induction time). Turnover frequencies of all samples are displayed in Fig. 4. Following the trend of the specific rate constants, the pre-calcined catalyst has a considerably higher TOF than any of the calcined samples. The pre-calcined TOF is roughly 35% higher than the sample calcined with no hold and the no hold sample is 105% higher than the sample calcined for 15 min indicating that the sites on the catalyst calcined with no hold are fundamentally more active than those on the catalyst calcined for 15 min. TOF is primarily influenced by nanoparticle size where smaller nanoparticles typically exhibit higher fundamental catalytic activity [57]. It was hypothesized that as nanoparticle size increased the TOF would decrease as a result. Here, it is seen that while calcination does have a noticeable impact on the fundamental activity of surface sites, a statistically significant increase in nanoparticle size (i.e. from 60 min to 180 min calcinations) does not result in drastic reductions in activity. The large decrease in catalytic activity between the no hold and 15 min calcinations cannot be directly attributed to size changes as no statistically significant size changes occur in this region. It can be concluded, however, that the surface sites on the un-calcined sample are fundamentally more active than on any of the calcined samples.

Activation energy studies were performed in order to detect changes in surface chemistry after calcination (Fig. 5). Prior to calcination, the measured activation energy was 18.7 kJ/mol, which generally agrees with most literature sources [44,58,59]. After calcination, the activation energy decreases. The change in the number of surface sites would not cause a reduction in the activation energy, thus this decrease must be due to an additional change at the catalyst surface. While a decrease in activation energy is not responsible for decreased catalytic rates, these results demonstrate an additional effect of calcination on catalyst properties. The decrease in activation energy after calcination may be

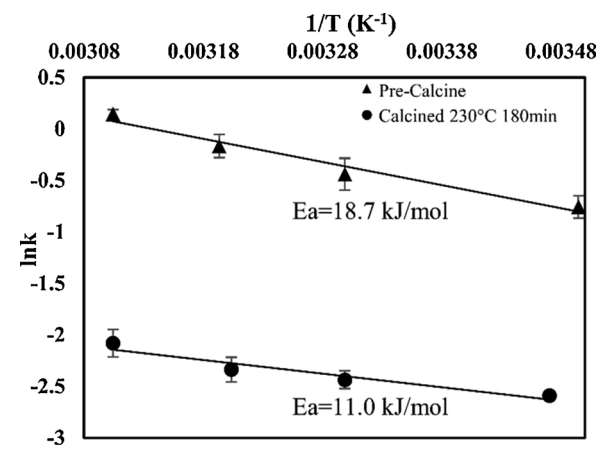


Fig. 5. Arrhenius plot of the pre-calcined and calcined 180 min samples.

due to rearrangements at the catalyst surface or may be due to the emergence of mass transport limitations. Based on a mass transfer limitation test in which activity tests were carried out at different stirring rates, (see Figure S4 of the Supporting Information) we are unable to definitively conclude which effect is responsible for the reduction in activation energy. However, it has been shown in the literature that hydrophilicity of the catalyst surface can affect catalytic activity as wettability is known to impact interactions between the catalyst and reactants [60].

During calcination, a portion of the APTES molecular species is removed as indicated by the ICP-MS and XPS results; as the hydrophilic molecular amine is removed from the silica, the surface becomes more hydrophobic. A hydrophilicity test shows that prior to calcination, the catalyst particles readily suspend in an aqueous phase while after a 180-minute calcination the particles preferentially remain in an organic phase, demonstrating the decreased hydrophilicity of the catalyst after partial removal of the molecular APTES (see Figure S5 of the Supporting Information). These results may suggest the emergence of mass transport limitations after calcination.

In addition to size changes, changes in surface hydrophilicity, and a change in activation energy, another interesting trend was observed during activity testing of the calcined samples. Prior to calcination, the hydrogenation reaction of 4-nitrophenol begins immediately upon addition of the catalyst with little to no induction time. After calcination, a small induction time became immediately apparent. Plots demonstrating the appearance of an induction time can be seen in Figure S6 of the Supporting Information. While the cause of this induction time is unknown without further investigation, a possible explanation is the rearrangement of surface atoms during calcination to minimize surface energy. It is suggested in the literature that one cause of the induction time is the dynamic restructuring of the nanoparticle surface into a geometry favorable for catalysis [61-63]. The calcined samples are potentially in a transitional state exhibiting unfavorable surface configurations leading to an induction time. While the observed overall reduction in catalytic activity cannot be directly attributed to any one of the changes demonstrated above, it is clear that calcination has an overall detrimental effect on catalyst properties and results in changes that typically are unaccounted for in traditional syntheses.

### 4. Conclusions

It was previously demonstrated that silylamine switchable surfactants can be used to synthesize and deposit nanoparticles on to a support surface while preserving monodispersity. Here, it is shown that upon reversal of the switchable surfactant to neutral form, nanoparticles are de-stabilized releasing surface-clean nanoparticles that can directly deposit on to a support material. Supported nanoparticle catalysts prepared in this manner do not require calcination for activation, as surface sites are completely bare after deposition as shown by XPS. While molecular APTES remains on the support surface, its presence does not appear to hinder catalytic activity. A low-temperature calcination cannot completely remove the APTES; however, here we are able to study the effects of calcination on bare nanoparticles. Unsurprisingly, calcination has an effect on nanoparticle size but further, even a lowtemperature calcination results in changes in surface hydrophilicity, catalyst activation energy, and the formation of an induction time. While calcination is commonly used as a method to remove bound surface molecules and activate catalysts, the detrimental effects of calcination on other catalyst properties are often completely overlooked. Traditionally, it has not been possible to effectively activate nanoparticles without the use of high-temperatures that alter the catalytic surface and, as such, there are potentially optimal surface arrangements that have not been accessed.

#### **Author contributions**

The manuscript was written through the contributions of all authors. All authors have given approval to the final version of the manuscript.

### **Funding sources**

This work was supported by the National Science Foundation under CBET-1651597 and institutional funding from Washington State University.

#### Acknowledgments

The authors thank the Franceschi Microscopy & Imaging Center, the Washington State University Center for NMR Spectroscopy, and Dr. Louis Scudiero for XPS assistance.

### Appendix A. Supplementary data

Supplementary material related to this article can be found, in the online version, at doi:https://doi.org/10.1016/j.apcata.2019.04.016.

#### References

- [1] C.B. Murray, C.R. Kagan, M.G. Bawendi, Annu. Rev. Mater. Sci. 30 (2000) 545–610, https://doi.org/10.1146/annurev.matsci.30.1.545.
- [2] T.K. Sau, A.L. Rogach, Adv. Mater. 22 (2010) 1781–1804, https://doi.org/10.1002/adma.200901271.
- [3] Y. Xia, Y. Xiong, B. Lim, S.E. Skrabalak, Angew. Chemie Int. Ed. 48 (2009) 60–103, https://doi.org/10.1002/anie.200890275.
- [4] A.R. Tao, S. Habas, P. Yang, Small 4 (2008) 310–325, https://doi.org/10.1002/ smll 200701295
- [5] J. Park, J. Joo, S.G. Kwon, Y. Jang, T. Hyeon, Angew. Chemie Int. Ed. 46 (2007) 4630–4660, https://doi.org/10.1002/anie.200603148.
- [6] B. Genorio, R. Subbaraman, D. Strmcnik, D. Tripkovic, V.R. Stamenkovic, N.M. Markovic, Angew. Chemie - Int. Ed. 50 (2011) 5468–5472, https://doi.org/10. 1002/anie.201100744.
- [7] G.A. Somorjai, H. Frei, J.Y. Park, J. Am. Chem. Soc. 131 (2009) 16589–16605, https://doi.org/10.1021/ja9061954.
- [8] G. Zhang, B. Xu, Nanoscale 2 (2010) 2798–2804, https://doi.org/10.1039/ CONR00295J.
- [9] R.W.J. Scott, O.M. Wilson, R.M. Crooks, J. Phys. Chem. B 109 (2005) 692–704, https://doi.org/10.1021/jp0469665.
- [10] Y. Wei, S. Han, J. Kim, S. Soh, B.A. Grzybowski, J. Am. Chem. Soc. 132 (2010) 11018–11020, https://doi.org/10.1021/ja104260n.
- [11] H. Lang, R.A. May, B.L. Iversen, B.D. Chandler, J. Am. Chem. Soc. 125 (2003) 14832–14836, https://doi.org/10.1021/ja0364120.
- [12] C.A. Witham, W. Huang, C. Tsung, J.N. Kuhn, G.A. Somorjai, F.D. Toste, Nat. Chem. 2 (2009) 36–41, https://doi.org/10.1038/NCHEM.468.
- [13] R.M. Crooks, M. Zhao, L.I. Sun, V. Chechik, L.E.E.K. Yeung, Acc. Chem. Res. 34 (2001) 181–190, https://doi.org/10.1021/ar000110a.
- [14] A. Villa, D. Wang, D. Shen Su, L. Prati, ChemCatChem 1 (2009) 510–514, https://doi.org/10.1002/cctc.200900118.
- [15] A.B.R. Mayer, J.E. Mark, Colloid Polym. Sci. 275 (1997) 333–340, https://doi.org/ 10.1007/s003960050090.
- [16] A. Quintanilla, V.C.L. Butselaar-Orthlieb, C. Kwakernaak, W.G. Sloof, M.T. Kreutzer, F. Kapteijn, J. Catal. 271 (2010) 104–114, https://doi.org/10.1016/ ii.ws.2010.03.01
- [17] L.D. Menard, F. Xu, R.G. Nuzzo, J.C. Yang, J. Catal. 243 (2006) 64–73, https://doi. org/10.1016/j.icat.2006.07.006.
- [18] G. Martra, L. Prati, C. Manfredotti, S. Biella, M. Rossi, S. Coluccia, J. Phys. Chem. B 107 (2003) 5453–5459, https://doi.org/10.1021/jp0225166.
- [19] J. Xian, Q. Hua, Z. Jiang, W. Huang, Langmuir 28 (2012) 6736–6741, https://doi. org/10.1021/la300786w.
- [20] D. Fenske, P. Sonstrçm, J. Stçver, X. Wang, H. Borchert, J. Parisi, J. Kolny-Olesiak, M. Baumer, K. Al-Shamery, ChemCatChem 2 (2010) 198–205, https://doi.org/10. 1002/cctc.200900232.
- [21] Q. Hua, T. Cao, X. Gu, J. Lu, Z. Jiang, X. Pan, L. Luo, W. Li, W. Huang, Angew. Chem.- Int. Ed. Ed. 53 (2014) 4856–4861, https://doi.org/10.1002/ange. 201402374.
- [22] J.Y. Park, C. Aliaga, J.R. Renzas, H. Lee, G.A. Somorjai, Catal. Lett. 129 (2009) 1–6, https://doi.org/10.1007/s10562-009-9871-8.
- [23] Y. Borodko, S.E. Habas, M. Koebel, P. Yang, H. Frei, G.A. Somorjai, J. Phys. Chem. B 110 (2006) 23052–23059, https://doi.org/10.1021/jp063338+.
- [24] P. Munnik, P.E. de Jongh, K.P. de Jong, Chem. Rev. 115 (2015) 6687–6718, https://doi.org/10.1021/cr500486u.
- [25] S. Tsubota, T. Nakamura, K. Tanaka, M. Haruta, Catal. Lett. 56 (1998) 131-135,

- https://doi.org/10.1023/A:1019069315071.
- [26] A.V. Neimark, L. Kheifez, V.B. Fenelonov, Ind. Eng. Chem. Prod. Res. Dev. 20 (1981) 439–450, https://doi.org/10.1021/i300003a006.
- [27] A. Lekhal, B.J. Glasser, J.G. Khinast, Chem. Eng. Sci. 56 (2001) 4473–4487, https://doi.org/10.1016/S0009-2509(01)00120-8.
- [28] J.A. Lopez-Sanchez, N. Dimitratos, C. Hammond, G.L. Brett, L. Kesavan, S. White, P. Miedziak, R. Tiruvalam, R.L. Jenkins, A.F. Carley, D. Knight, C.J. Kiely, G.J. Hutchings, Nat. Chem. 3 (2011) 551–556, https://doi.org/10.1038/NCHEM. 1066.
- [29] J. Kilmartin, R. Sarip, R. Grau-Crespo, D. Di Tommaso, G. Hogarth, C. Prestipino, G. Sankar, ACS Catal. 2 (2012) 957–963, https://doi.org/10.1021/cs2006263.
- [30] T.R. Gordon, M. Cargnello, T. Paik, F. Mangolini, R.T. Weber, P. Fornasiero, C.B. Murray, J. Am. Chem. Soc. 134 (2012) 6751–6761, https://doi.org/10.1021/ is300823a
- [31] E.W. Elliott, R.D. Glover, J.E. Hutchison, ACS Nano 9 (2015) 3050–3059, https://doi.org/10.1021/nn5072528.
- [32] L. Cademartiri, A. Ghadimi, G.A. Ozin, Acc. Chem. Res. 41 (2008) 1820–1830, https://doi.org/10.1021/ar800158d.
- [33] J.R. Vig, J. Vac. Sci. Technol. Vacuum, Surf., Film 3 (1985) 1027, https://doi.org/ 10.1116/1.573115.
- [34] L.R. Baker, G. Kennedy, J.M. Krier, M. Van Spronsen, R.M. Onorato, G.A. Somorjai,
- Catal. Lett. 142 (2012) 1286–1294, https://doi.org/10.1007/s10562-012-0904-3. [35] C. Aliaga, J.Y. Park, Y. Yamada, H.S. Lee, C. Tsung, P. Yang, G.A. Somorjai, J. Phys.
- Chem. C 113 (2009) 6150-6155, https://doi.org/10.1021/jp8108946.

  [36] J.M. Krier, W.D. Michalak, L.R. Baker, K. An, K. Komvopoulos, G.A. Somorjai, J. Phys. Chem. C 116 (2012) 17540-17546, https://doi.org/10.1021/jp303363m
- Phys. Chem. C 116 (2012) 17540–17546, https://doi.org/10.1021/jp303363m.
  [37] L.R. Baker, M. Van Spronsen, A. Hervier, X. Cai, S. Chen, L. Wang, G.A. Somorjai, J.
- Am. Chem. Soc. 134 (2012) 14208–14216, https://doi.org/10.1021/ja306079h.
   [38] C.J. Kliewer, C. Aliaga, M. Bieri, W. Huang, C. Tsung, J.B. Wood, K. Komvopoulos, G.A. Somorjai, J. Am. Chem. Soc. 132 (2010) 13088–13095, https://doi.org/10.1021/ja105800z.
- [39] Y. Yamada, C. Tsung, Z. Huang, S. Habas, T. Soejima, C. Aliaga, G. Somorjai, P. Yang, Nat. Chem. 3 (2011) 372–376, https://doi.org/10.1038/NCHEM.1018.
- [40] C.H. Bartholomew, Appl. Catal. A Gen. 212 (2001) 17–60, https://doi.org/10. 1016/S0926-860X(00)00843-7.
- [41] Z. Niu, Y. Li, Chem. Mater. 26 (2014) 72-83 0.1021/cm4022479.
- [42] K. Bryant, G. Ibrahim, S.R. Saunders, Langmuir 33 (2017) 12982–12988, https://doi.org/10.1021/acs.langmuir.7b02983.
- [43] A.L. Ethier, E.C. Hart, S.R. Saunders, E.J. Biddinger, A.Z. Fadhel, C. Dilek, P. Pollet, C. a Eckert, C.L. Liotta, Green Mater. 2 (2014) 54–61, https://doi.org/10.1680/ gmat.13.00020.
- [44] K. Kuroda, T. Ishida, M. Haruta, J. Mol. Catal. A: Chem. 298 (2009) 7-11, https://

- doi.org/10.1016/j.molcata.2008.09.009.
- [45] J.W. Tukey, Biometrics 5 (1949) 99–114, https://doi.org/10.2307/3001913.
  [46] W. Xie, J. Chen, J. Agric. Food Chem. 62 (2014) 10414–10421, https://doi.org/10.1021/jf503726a.
- [47] L. Garcia, M.L. Salvador, R. Bilbao, J. Arauzo, Energy Fuels 12 (1998) 139–143, https://doi.org/10.1021/ef970097j.
- [48] S.G. Agalave, M.B. Chaudhari, G.S. Bisht, B. Gnanaprakasam, ACS Sustainable Chem. Eng. 6 (2018) 12845–12854, https://doi.org/10.1021/acssuschemeng. 8b02090
- [49] G. Yang, W. Chang, D.T. Hallinan, J. Colloid Interface Sci. 460 (2015) 164–172, https://doi.org/10.1016/j.jcis.2015.08.054.
- [50] M. Bhat, J. Ahn, D.L. Kwong, M. Arendt, J.M. White, Appl. Phys. Lett. 64 (1994) 1168–1170, https://doi.org/10.1063/1.111951.
- [51] E.T. Kang, K.G. Neoh, Z.H. Ma, K.L. Tan, Colloid Polym. Sci. 279 (2001) 73–76, https://doi.org/10.1007/s003960000418.
- [52] G.V. Soares, K.P. Bastos, R.P. Pezzi, L. Miotti, C. Driemeier, I.J.R. Baumvol, C. Hinkle, G. Lucovsky, Appl. Phys. Lett. 84 (2004) 4992–4994, https://doi.org/10. 1063/1.1763230
- [53] M. Aslam, L. Fu, M. Su, K. Vijayamohanan, V.P. Dravid, J. Mater. Chem. 14 (2004) 1795–1797, https://doi.org/10.1039/B402823F.
- [54] H. Shimizu, H. Wakashima, S. Shimada, T. Ishikawa, M. Ikeda, Surf. Interface Anal. 40 (2008) 627–630, https://doi.org/10.1002/sia.2629.
- [55] K. Asami, J. Electron Spectros. Relat. Phenomena 9 (1976) 469–478, https://doi. org/10.1016/0368-2048(76)80065-5.
- [56] E. Varga, P. Pusztai, A. Oszko, K. Baan, A. Erdohelyi, Z. Konya, J. Kiss, Langmuir 32 (2016) 2761–2770, https://doi.org/10.1021/acs.langmuir.5b04482.
- [57] S. Panigrahi, S. Basu, S. Praharaj, S. Pande, S. Jana, A. Pal, S.K. Ghosh, T. Pal, J. Phys. Chem. C 11 (2007) 4596–4605, https://doi.org/10.1021/jp067554u.
- [58] S. Gu, S. Wunder, Y. Lu, R. Fenger, K. Rademann, B. Jaquet, A. Zaccone, M. Ballauff, J. Phys. Chem. C 118 (2014) 18618–18625, https://doi.org/10.1021/jp5060606.
- [59] T. Ma, W. Yang, S. Liu, H. Zhang, F. Liang, Catalysts 7 (2017) 38, https://doi.org/ 10.3390/catal7020038.
- [60] X. Chen, P. Qian, T. Zhang, Z. Xu, C. Fang, X. Xu, W. Chen, P. Wu, Y. Shen, S. Li, J. Wu, B. Zheng, W. Zhang, F. Huo, Chem. Commun. 54 (2018) 3936–3939, https://doi.org/10.1039/C8CC00318A.
- [61] S. Gu, S. Wunder, Y. Lu, M. Ballau, R. Fenger, K. Rademann, B. Jaquet, A. Zaccone, J. Phys. Chem. C 118 (2014) 18618–18625, https://doi.org/10.1021/jp5060606.
- [62] X. Zhou, W. Xu, G. Liu, D. Panda, P. Chen, J. Am. Chem. Soc. 132 (2010) 138–146, https://doi.org/10.1021/ja904307n.
- [63] W. Xu, J.S. Kong, Y.E. Yeh, P. Chen, Nat. Mater. 7 (2008) 992–996, https://doi.org/ 10.1038/nmat2319.